Available online at www.sciencedirect.com

ScienceDirect

Procedia Computer Science 267 (2025) 4–13

Procedia Computer Science

www.elsevier.com/locate/procedia

Proceedings of the Third EuroHPC user day

The QCD crossover line in a finite volume

Szabolcs Borsányi[a,*], Zoltán Fodor[b,a,c,d], Jana N. Guenther[a], Paolo Parotto[e], Attila Pásztor[c], Ludovica Pirelli[a], Kálmán K. Szabó[a,d], Chik Him Wong[a]

[a] *Department of Physics, Wuppertal University, Gaussstr. 20, D-42119, Wuppertal, Germany*
[b] *Pennsylvania State University, Department of Physics, State College, PA 16801, USA*
[c] *Institute for Theoretical Physics, ELTE Eötvös Loránd University, Pázmány P. sétány 1/A, H-1117 Budapest, Hungary*
[d] *Jülich Supercomputing Centre, Forschungszentrum Jülich, D-52425 Jülich, Germany*
[e] *Dipartimento di Fisica, Università di Torino and INFN Torino, Via P. Giuria 1, I-10125 Torino, Italy*

Abstract

We compute the crossover line of strongly interacting matter in the temperature (T) – baryo-chemical potential (μ_B) plane of the QCD phase diagram. We use large scale lattice QCD simulations at vanishing μ_B to solve the path integral in the transition regime between $T = 120$ and 200 MeV. We introduce a high order Taylor scheme for the Polyakov loop and extract the static quark entropy. The peak position of the latter defines the transition line that we can extract up to 400 MeV in μ_B. For the simulations the 4HEX staggered action was used with 2+1 flavors at physical quark masses.

Keywords: Lattice QCD ; QCD phase diagram

1. Introduction

Vacuum heated to the extreme temperatures of $\sim 10^{12}$ K turns into a new phase where matter and antimatter and their force carriers form a fluid, the Quark Gluon Plasma (QGP). As its name suggests quark fields constitute the matter component and gluons mediate their interaction. If we increase the temperature, interactions between quarks weaken, if we lower the temperature quarks and antiquarks will be confined into hadrons and anti-hadrons, respectively, forming a weakly interacting gas of baryons and mesons without visible gluonic terms. The transition from QGP to the hadronic phase has actually happened in our Universe when it was ~ 10 μs old. The same transition has been reproduced several billion times in the Large Hadron Collider (LHC) at CERN as well as in the Relativistic Heavy Ion Collider (RHIC) at the Brookhaven National Lab (BNL).

There is ample experimental evidence for this transition being an analytical crossover [1, 2, 3]. Theory has predicted the crossover nature of the transition [4]. In fact, one can apply statical field theory methods to solve the path

* Corresponding author. Tel.: +49-202-439-2635
E-mail address: borsanyi@uni-wuppertal.de

1877-0509
10.1016/j.procs.2025.08.229

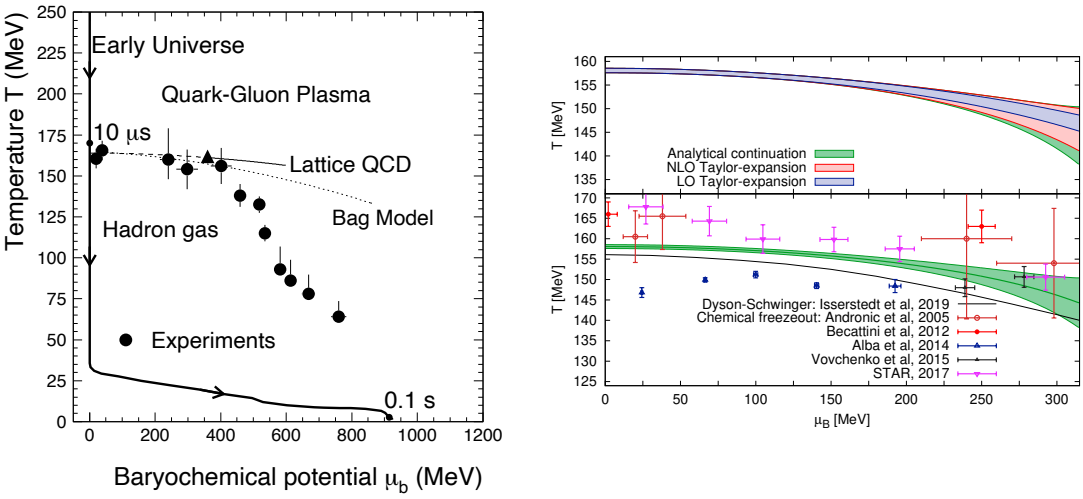

Fig. 1. The QCD phase diagram in the $T - \mu_B$ plane. Left: a version from 2008 [8], right: our recent continuum extrapolated lattice result [9]. The data points refer to the chemical freeze-out line in both figures. The green band on the right plot is our lattice result, the other lines refer to various theoretical approaches.

integral of Quantum Chromodynamics (QCD) the underlying theory to strong interactions. Lattice QCD, a computational discipline within theoretical high energy physics, can implement importance sampling to generate field configurations with the weight given by the Euclidean quantum field theory. With such lattice simulations the central temperature of the crossover has been determined to be $T \approx 155$ MeV [5, 6].

The beam energy in collision experiments controls the baryon stopping and through that the excess of quarks over antiquarks in the plasma. This gave the opportunity for a Beam Energy Scan (BES) program at RHIC, where the transition could be studied as a function of net baryon density. However, lattice simulations struggle with an asymmetric setup between matter and antimatter. Most theoretical frameworks introduce a baryo-chemical potential μ_B as the free energy associated with the shifting of the balance by three quarks. While for vanishing values of μ_B the statistical weight of the field configurations are real and positive, allowing for a stochastic process to sample it, lattice QCD faces with complex probabilities whenever a grand canonical simulation with non-zero μ_B is asked for. Though it is possible to restrict the simulation to the real part based on exact cancellation of the imaginary part, the physics result is encoded in the approximate cancellation of large positive and negative real contributions [7]. This is called the sign problem in finite density lattice QCD. It does not immediately make simulations at finite μ_B impossible, but drives the costs exponentially high both in μ_B^2 and in the system size.

Given the rich experimental program at RHIC and the future CBM experiment at FAIR the theory community is challenged to make reliable predictions for finite density QCD near its crossover temperature. One key feature in the $T - \mu_B$ phase diagram is the transition line (see Fig. 1). We already know from lattice simulations that it starts at the temperature axis ($\mu_B = 0$) as a crossover at $T \approx 155$ MeV.

The data points in Fig. 1 refer to experimental observations of the collision outcome. Particle abundances are matched against a thermal model based on the grand canonical parameters T and μ_B. These are the chemical freeze-out parameters and reflect the temperature of the matter at the moment of the last inelastic scattering. While the underlying model assuming an instantaneous disintegration of the thermal plasma may seem oversimplified, it is very successful in the description of the particle yields and gives results close to lattice transition line [10].

Our earlier lattice result in Fig. 1 is based on the analytical continuation method [11, 12]. It exploits that for imaginary valued chemical potentials the weight of individual lattice configurations are still real and positive, allowing importance sampling to work for $\mu_B^2 < 0$. The transition temperatures were determined for several fixed negative $(\mu_B/T)^2$ values and were extrapolated to the physical side with $\mu_B^2 > 0$. The crossover line was first computed in the continuum limit in Ref. [13].

Fig. 1 also shows an abrupt change of the chemical freeze-out line near $\mu_B \approx 400$ MeV. It is not clear, whether the lattice extrapolation breaks down, the thermal model's assumptions are no longer valid, or there is a highly compressed hadronic phase above the chemical freeze-out line. This region will be explored in detail by the CBM experiment in the near future.

It is reasonable to assume that the crossover line may turn in to a first order line separated by a critical end-point. If it happens, fluctuation measurements of net baryon (or proton) density will show a possibly large non-monotonic signal as a function of beam energy [14]. One of the science goals of the Beam Energy Scan program of the STAR experiment was to find these. As it happens, Nature has placed the critical endpoint outside of STAR's range [15].

The intense experimental research has stimulated significant developments in the theoretical frameworks. While lattice QCD was experimenting with novel ways to extrapolate or directly simulate at finite μ_B, diagrammatic approaches, such as the Dyson-Schwinger method [16] and similar ways based on the functional renormalization group [17] have delivered promising results.

Our work presented in this paper is motivated by the urgent need to follow up on the crossover line and search for the signatures of criticality. In section 2 we start with the role of the simulation volume and outline the simulation strategy in 3. After presenting various cross-checks in section 4 we present a new result on the transition line in section 5. We finally discuss further planned use of the generated data in section 6.

2. Simulation volume and the sign problem

A popular and successful method to extract finite density information from simulations that were run at $\mu_B = 0$ is to compute Taylor expansion coefficients. To illustrate this we consider the pressure, normalized to temperature

$$\left.\frac{p}{T^4}\right|_{T,\mu_B} = \left.\frac{p}{T^4}\right|_{T,0} + \frac{\hat{\mu}_B^2}{2!}\chi_2(T) + \frac{\hat{\mu}_B^4}{4!}\chi_4(T) + \frac{\hat{\mu}_B^6}{6!}\chi_6(T) + \dots \tag{1}$$

where the coefficients themselves are highly complex lattice observables. We used the shorthand $\hat{\mu} = \mu/T$. For instance, $\chi_2(T)$ is obtained as the variance of the quark number on the configurations, as dictated by the fluctuation-response theorem.

What we call a lattice configuration contains the bosonic fields (gluons) only. The fermionic part (quarks) is quadratic and can be integrated out leaving us with a non-local bosonic theory that we actually simulate. To extract variance, kurtosis or even higher moments of the quark number (for χ_6) we have to revisit the fermionic contribution and find out the Taylor expansion for each configuration U. Since the quark contribution is a determinant, $\det M(U,\mu)$, its expansion can be written as

$$\begin{aligned}\log\det M_j^{1/4}(U,m_j,\mu_j) = \log\det M_j^{1/4}(U,m_j,0) + A_j\hat{\mu}_j \\ + \frac{1}{2!}B_j\hat{\mu}_j^2 + \frac{1}{3!}C_j\hat{\mu}_j^3 + \dots\end{aligned} \tag{2}$$

Notice, that wile charge conjugation symmetry forbids the odd term on the level of a physical observable, such as the pressure, Eq. (2) is not protected. In Eq. (2) we introduced a separate chemical potential for each quark flavor, since their numbers are conserved separately. Dropping the flavor index for simplicity we find for the first few orders

$$\begin{aligned}
\chi_2 &= +\langle B\rangle + \langle AA\rangle \\
\chi_4 &= +\langle D\rangle + 3\langle BB\rangle - 3\langle B\rangle\langle B\rangle + 4\langle AC\rangle + \langle AAAA\rangle - 3\langle AA\rangle\langle AA\rangle + 6\langle AAB\rangle - 6\langle B\rangle\langle AA\rangle \\
\chi_6 &= +\langle F\rangle + 10\langle CC\rangle + 15\langle BD\rangle + 15\langle BBB\rangle + 6\langle AE\rangle + 60\langle ABC\rangle + 15\langle AAD\rangle \\
&\quad +45\langle AABB\rangle + 20\langle AAAC\rangle + 15\langle AAAAB\rangle + \langle AAAAAA\rangle - 15\langle D\rangle\langle B\rangle \\
&\quad -15\langle D\rangle\langle AA\rangle - 45\langle B\rangle\langle BB\rangle - 60\langle B\rangle\langle AC\rangle - 90\langle B\rangle\langle AAB\rangle \\
&\quad -15\langle B\rangle\langle AAAA\rangle - 45\langle BB\rangle\langle AA\rangle - 60\langle AC\rangle\langle AA\rangle - 90\langle AA\rangle\langle AAB\rangle \\
&\quad -15\langle AA\rangle\langle AAAA\rangle + 30\langle B\rangle\langle B\rangle\langle B\rangle + 90\langle B\rangle\langle B\rangle\langle AA\rangle \\
&\quad +90\langle B\rangle\langle AA\rangle\langle AA\rangle + 30\langle AA\rangle\langle AA\rangle\langle AA\rangle \\
\chi_8 &= 79 \text{ terms} \dots
\end{aligned}$$

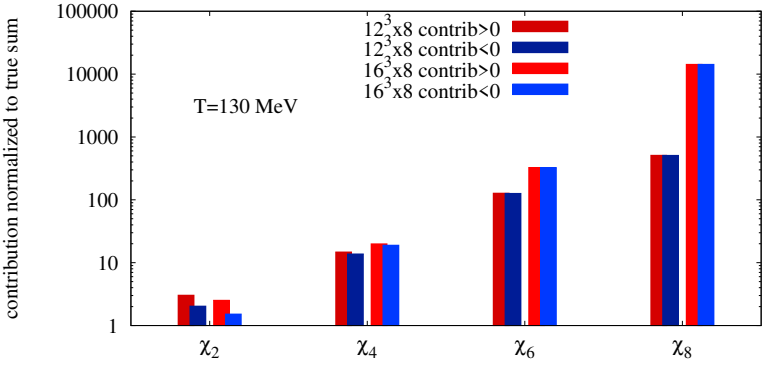

Fig. 2. Remnant sign problem in the Taylor coefficients of the finite-μ_B extrapolation for two volumes. We show the sum of positive and negative contributions as two bars, their difference is the actual value of χ_n. With every new order the signal-to-noise ratio deteriorates with a volume-dependent factor.

High orders in μ_B (where all quarks flavors are considered) are very tedious to obtain. We developed a computer algebra system to compute these and to act as a code generator. The biggest problem, however, is not computational complexity, but the cancellation between positive and negative contributions within the expressions for χ_n. This is a remnant of the finite density sign problem (see Fig. 2).

It is clear from Fig. 2 that large simulation volumes turn the high order extrapolation schemes impractical. Past lattice studies have often used large volumes e.g. $32^3 \times 8$, then even extreme statistics could not reduce the large statistical error on χ_6 and χ_8 [18]. In our recent work we started with the much smaller $16^3 \times 8$ simulation size and could compute the high orders in the continuum limit [19].

But before we proceed with a small system size to obtain the crossover line we have to find answer two very practical questions: which observable can be used to identify the transition temperature in a small volume, and how can this be extrapolated to finite density?

The first question we addressed in Ref. [20]. In Fig. 3 we show the main result. We investigated five different observables and plotted the transition temperature as a function of the volume (at vanishing μ_B). Three of these observables are based on chiral observables ($\chi_{\text{full}}, \chi_{\text{disc}}$ and pbp for $\langle\bar{\psi}\psi\rangle$), two are related to the Polyakov loop as

$$F_Q = -T \log\left(\frac{1}{V}\sum_{\vec{x}} |\langle P(\vec{x})\rangle_T|\right) \tag{3}$$

$$S_Q = -\frac{\partial F_Q}{\partial T}, \tag{4}$$

where $P(\vec{x})$ is the Polyakov loop

$$P(\vec{x}) = \frac{1}{3}\mathrm{Tr}\prod_{x_4=0}^{N_t-1} U_4(\vec{x}, x_4), \tag{5}$$

the $U_\mu(\vec{x}, x_4)$ are the usual link variables in lattice gauge theory.

In this work we focus on the Polyakov loop and the $S_Q(T)$ observable.

3. Transition temperature at finite density

Our next task is to compute $S_Q(T)$ at finite μ_B. For this we will work out the Taylor series of the real and imaginary parts of the Polyakov loop and through that we will find the expansion coefficients of $F_Q(T)$. We will use these to obtain $F_Q(T, \mu_B)$ to eight order and find the crossover temperature by finding its inflection point.

We start by defining the chain rule for an arbitrary variable X. Following Ref. [21] we have:

$$\partial_j \langle X\rangle = \left\langle XA_j\right\rangle - \langle X\rangle\left\langle A_j\right\rangle + \left\langle \partial_j X\right\rangle, \tag{6}$$

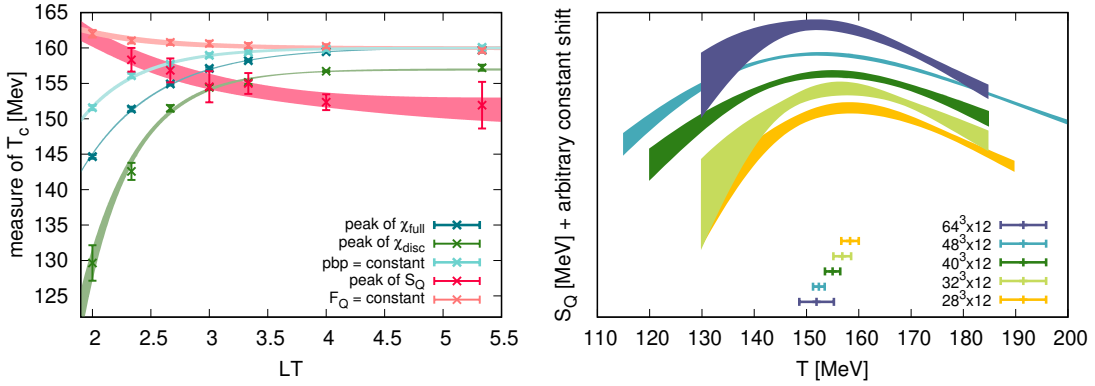

Fig. 3. Left: Five observables that can be used as a proxy for the transition temperature. Right: The static quark entropy exhibits a peak at the transition. The volume dependence is mild. (Plots from Ref. [20]).

$$\begin{aligned}\partial_k\partial_j\langle X\rangle = &\frac{1}{2}\left\langle XA_jA_k\right\rangle - \frac{1}{2}\langle X\rangle\left\langle A_jA_k\right\rangle - \left\langle XA_j\right\rangle\langle A_k\rangle\\ &+\langle X\rangle\langle A_k\rangle\left\langle A_j\right\rangle + \left\langle(\partial_k X)A_j\right\rangle - \langle\partial_k X\rangle\langle A_k\rangle\\ &+\frac{1}{2}\left\langle\partial_k\partial_j X\right\rangle - \frac{1}{2}\langle X\rangle\left\langle\partial_k A_j\right\rangle\\ &+(j\leftrightarrow k)\,.\end{aligned} \tag{7}$$

where ∂_j stands for $\partial/\partial\hat{\mu}_j$ and we used a flavor-specific coefficients $A_j, B_j, \ldots$ for the quark determinant $\det M_j(T,\mu_j)$. These directly yield the derivatives

$$\partial_j\langle P_R\rangle\big|_{\mu\equiv 0} = 0\,, \tag{8}$$

$$\partial_j\langle P_I\rangle\big|_{\mu\equiv 0} = \left\langle A_jP_I\right\rangle\,, \tag{9}$$

$$\begin{aligned}\partial_j\partial_k\langle P_R\rangle\big|_{\mu\equiv 0} = &\,\delta_{jk}\left[\left\langle B_jP_R\right\rangle - \left\langle B_j\right\rangle\langle P_R\rangle\right]\\ &\left\langle A_jA_kP_R\right\rangle - \left\langle A_jA_k\right\rangle\langle P_R\rangle\,,\end{aligned} \tag{10}$$

$$\partial_j\partial_k\langle P_I\rangle\big|_{\mu\equiv 0} = 0\,. \tag{11}$$

or for F_Q one can work out the expansion scheme

$$F = -\frac{T}{2}\log|\langle P\rangle|^2 = T\sum_{n=0,2,\ldots}\frac{F_n}{n!}\left(\frac{\mu}{T}\right)^n \tag{12}$$

$$F_0 = -\frac{1}{2}\log(Q) \tag{13}$$

$$F_2 = -\frac{1}{2}\left[+\frac{Q^{(2)}}{Q}\right] \tag{14}$$

For higher orders we used a code generator. The complete list of formulas can be found in Ref. [22]. We show the resulting coefficients as a function of temperature in Fig. 4.

Fig. 4 shows the results for two different expansion schemes. The red data points represent our results in the straightforward μ_B expansion scheme. The blue points also refer to coefficients in μ_B, however, in that case the strangeness chemical potential μ_S is tuned order-by-order such that the resulting strangeness density vanishes in the complete parameter range. The latter setup is the closest to the experimentally studied case, and it was already used in Fig. 1.

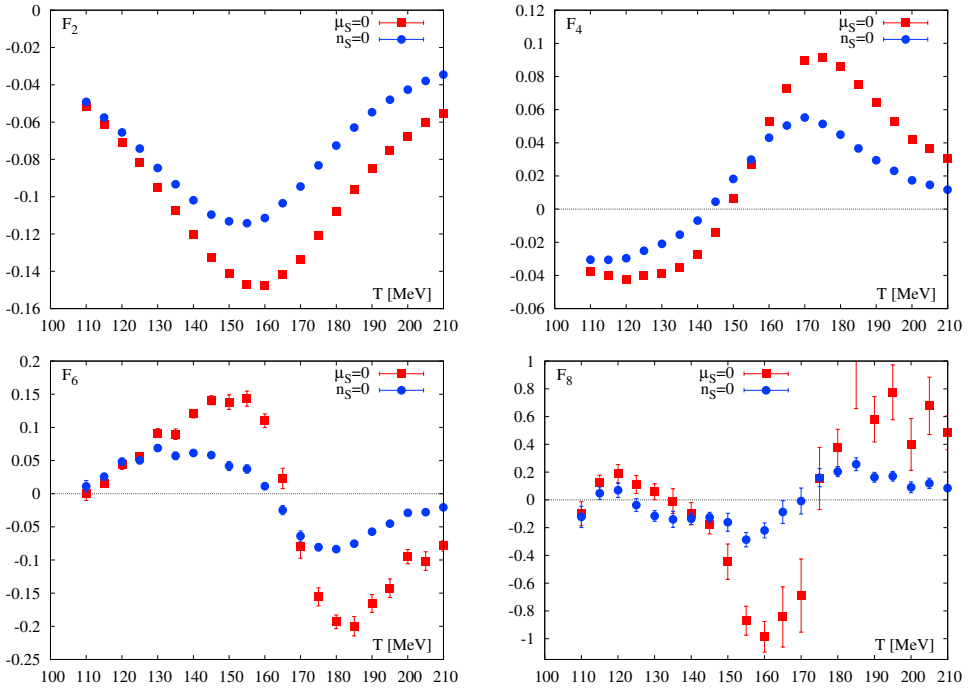

Fig. 4. Taylor coefficients of the static quark free energy in two setups: vanishing strangeness chemical potential in red, along strangeness neutral trajectories in blue (Updated version of the original plots in Ref. [22])

4. Validity of the extrapolation

To check the validity of the extrapolation we compare our extrapolated results to direct simulation data. As we have already mentioned, simulations with negative μ_B^2 are technically possible and we supplemented our data set with such runs so that such a comparison can be made.

In the following we will use the already determined expansion coefficients and insert negative μ_B^2 in the Taylor formula. We plot the resulting real and imaginary parts of the Polyakov loop against direct data in Fig. 5.

As an additional check we compute the bare $F_Q(\mu_B)$ for imaginary chemical potentials. This quantity requires renormalization, but this only applies a constant shift to $F_Q(\mu_B)$, it plays no role for this comparison. In order to obtain direct data along the strangeness neutral line at imaginary μ_B, we performed a reweighting of each Im $\mu_B > 0$ ensemble to the specific imaginary μ_S where $n_S = 0$. The target $\mu_S(\mu_B)$ was also computed using reweighting, with reweighting factors spread between 0.5 and 2. Even in the $n_S = 0$ scheme, our error bars are smaller than the symbol size. We stress that reweighting was only applied to the imaginary μ_B data and only for the sake of this crosscheck. We will refer to the resulting F_Q for both schemes as direct data, as opposed to the Taylor expansion, that is based on the $\mu_B = 0$ ensemble. We show the comparison in the right panel of Fig. 5.

5. A new estimate for the crossover line

We start with the presentation of the renormalized Polyakov loop, since most readers are more familiar with this observable than F_Q or S_Q. Since we have already established F_Q at finite μ_B we define the renomalized Polyakov loop as $P^r = \exp -(F_Q - \Delta)/T$, where Δ sets the scheme. This means that for observables in this paper we always expand F_Q, not P_R or P_I. We choose Δ such that $P^r(T = 160\ \text{MeV}, \mu_B = 0) = 1$ as we did in Ref. [20]. The Polyakov loop curves are shown in Fig. 6. In the bottom panel of this figure, we also show the fourth, sixth and eighth order curves for $T = 130$ MeV. The expansion is under control below $\mu_B \approx 400$ MeV.

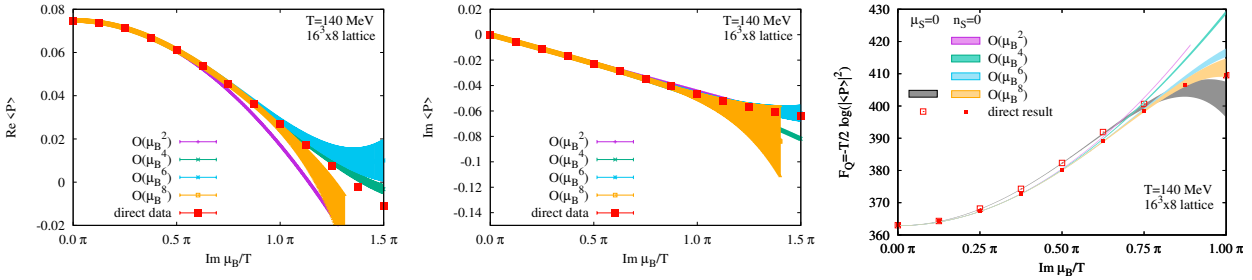

Fig. 5. The Taylor coefficients are used to extrapolate the bare Polyakov loop expectation value from $\mu_B = 0$ to imaginary values of the baryochemical potential. (Left: real part, Middle: imaginary part, Right: the resulting static quark potential F_Q) We demonstrate the convergence of the series at $T = 140$ MeV by comparing orders of the extrapolations (bands) to directly measured expectation values at Im $\mu_B > 0$ from a separate set of simulations. In the right plot we show two comparisons, one in the $\mu_S = 0$ scheme, and one in the strangeness netural $n_S = 0$ case.

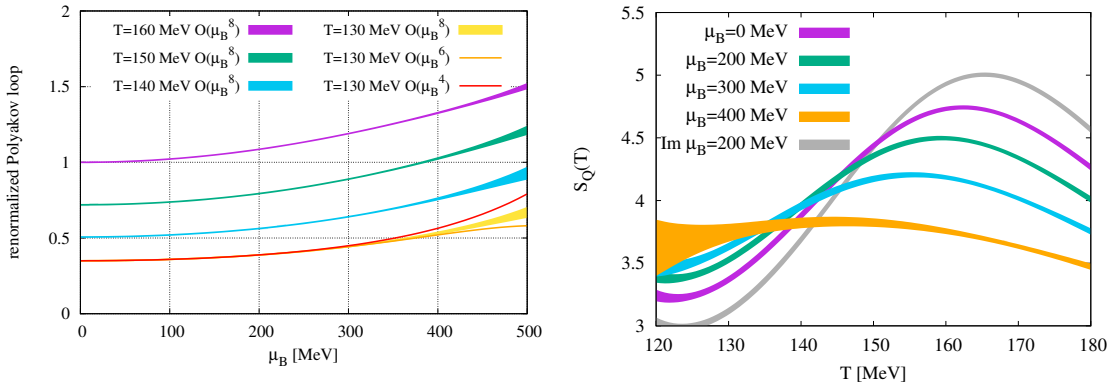

Fig. 6. Left: The Polyakov loop shown as a function of μ_B with fixed T. For one of the temperatures we show the fourth and sixth order results. The sixth order does not visibly differ from the full computation below $\mu_B = 350$ MeV. Right: The static quark entropy ($S_Q(T)$) extrapolated to various chemical potentials. The errors in this plot are statistical only. We added one imaginary chemical potential (gray band) to better visualize the trend in μ_B.

In the right panel of Fig. 6 we show $S_Q(T)$ as defined in Eq. (4). We also show $S_Q(T)$ for one imaginary value of μ_B for comparison. The $S_Q(T)$ curves show two trends very clearly. First, the change in the peak position indicates the chemical potential dependence of the transition temperature. Second, the width of the peak increases as μ_B grows, indicating a weakening of the deconfinement transition. At the largest value of μ_B, the curve is the flattest. This feature contributes to the difficulty in determining the deconfinement temperature at large μ_B, in addition to the growing errors from the extrapolation. On the other hand, in the opposite (imaginary) direction, the peak is higher and narrower, eventually becoming singular in the Roberge-Weiss point [23].

Our final results are the deconfinement transition temperature and the width of the deconfinement transition as a function of the chemical potential. For the strangeness neutral case they are shown in Fig. 7. On the left, the deconfinement crossover temperature calculated in this work is compared to the chiral crossover temperature from Ref. [9] and an estimate of the freeze-out parameters in heavy ion collisions by the STAR collaboration [25] and the parametrization in Ref. [10]. On the right we show the chiral transition width from Ref. [9] and the deconfinement width from this work. Already at $\mu_B = 0$ the deconfinement transition is much broader. Even more interestingly, as a function of the baryochemical potential, the deconfinement transition broadens, while the width of the chiral transition stays roughly the same. This contrasting behaviour was already observed in our earlier work [20], but only to leading order in μ_B. Here, we observe the same behavior in a large range of chemical potential. Our results disfavor the existence of a deconfinement critical endpoint below $\mu_B \approx 400$MeV. The same statement is also true for zero strangeness chemical potential. However, in that setup, we see the reverse trend of the width. Above $\mu_B \approx 300$MeV the width of the

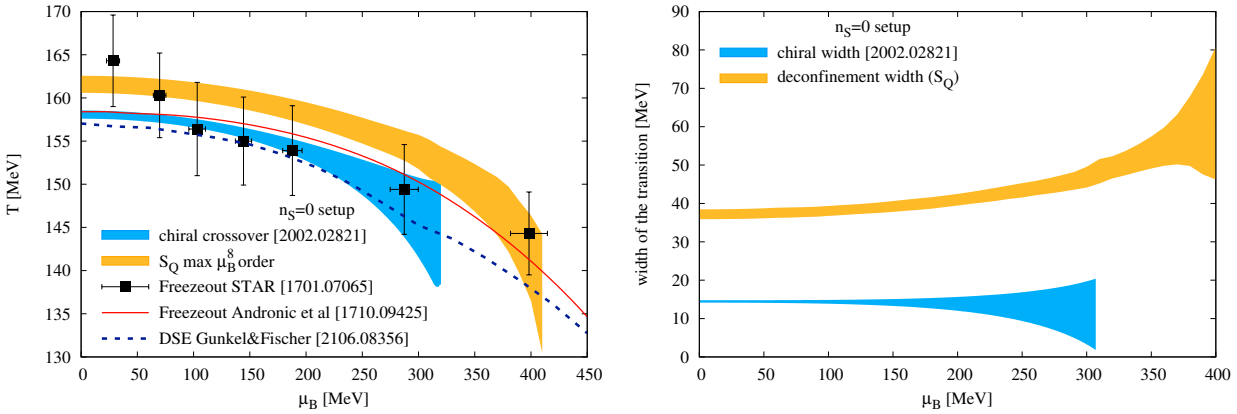

Fig. 7. Left: the deconfinement line (orange) defined as the peak position of the static quark entropy (S_Q) at fixed μ_B as a function of μ_B. We add the chiral transition line from lattice QCD [9] in the phase diagram, defined from the peak of the full chiral susceptibility, as well as the corresponding result based on Dyson-Schwinger equations [24] (the latter used the $\mu_S = \mu_B/3$ scheme as an approximation to $n_S = 0$). We also include the chemical freeze-out parameters [25, 10]. Right: the width associated to the deconfinement (orange) and chiral (blue) transitions: the two differ already at $\mu_B = 0$. With increasing μ_B, while the chiral width is mostly constant, the deconfinement width grows.

deconfinement transition gets smaller again. This is what one expects if a critical endpoint exists somewhere above $\mu_B = 400$MeV.

Finally, we address the robustness of the present computation. We use the eighth order of the Taylor series, which may seem a very arbitrary decision. In fact, the order of the expansion was only limited by the statistics. Up to 300 MeV the effect of the eighth order is invisible, and only gets statistically significant above $\mu_B \simeq 350$ MeV. For the $\mu_S = 0$ scheme the onset of the eighth order appears 50 MeV earlier. It is safe to claim that up to $\mu_B \leq 300$ MeV the systematic errors from the truncated extrapolation can be completely neglected, and we give a fair description of finite volume QCD at finite μ_B. At the same time, the eighth order is the lowest possible truncation in the range 300-400 MeV. Lower orders cannot give reliable results. The difference in the width between the $n_S = 0$ and $\mu_S = 0$ schemes is an effect that is visible only if the eighth order is included.

6. Outlook

The computational challenge in this work was twofold. First, it required a statistics of 1-2 million gauge configurations per temperature. The second half of the computer time was used for the measurements of the $A_j, B_j, C_j, \ldots$ coefficients. For this we used the reduced matrix formalism [26] that translates the problem of the μ_B dependence of the fermion determinant into an eigenvalue problem. We used the MAGMA library [27] to cope with the dense linear algebra problems on LUMI's accellerators.

While this was computation was very costly, having these eigenvalues we can, compute many other observables using the same configurations on the $16^3 \times 8$ lattice without much effort. Examples for future use of the data include:

i) We can compute the canonical determinants and rewrite the grand canonical ensemble as a canonical. This can give us access to the physics of small systems, relevant e.g. for proton-lead events.
ii) We can compute high order baryon fluctuations and use these to extrapolate the baryon kurtosis-to-variance ratio. This observable was measured by the STAR experiment for protons and is key in the search for the critical end point in the QCD phase diagram.
iii) Modelling the QCD grand canonical partition sum one can estimate the position of Lee-Yang zeros. These approach real values in the vicinity of the critical end-point with universal critical scaling.
iv) We can extend the range of fluctuation-based observables to strangeness. The statistical errors on strangeness fluctuations are significantly smaller, and the extrapolation up to 500 MeV is feasible with our statistics.

The data analysis for all these projects are currently underway and will deliver results in the second project year.

Acknowledgements

The project was supported by the BMBF Grant No. 05P21PXFCA. This work is also supported by the MKW NRW under the funding code NW21-024-A. Further funding was received from the DFG under the Project No. 496127839. This work was also supported by the Hungarian National Research, Development and Innovation Office, NKFIH Grant No. KKP126769. This work was also supported by the NKFIH excellence grant TKP2021_NKTA_64. This work is also supported by the Hungarian National Research, Development and Innovation Office under Project No. FK 147164. The authors gratefully acknowledge the Gauss Centre for Supercomputing e.V. (www.gauss-centre.eu) for funding this project by providing computing time on the GCS Supercomputer Juwels-Booster at Juelich Supercomputer Centre. We acknowledge the EuroHPC Joint Undertaking for awarding this project access to the EuroHPC supercomputer LUMI, hosted by CSC (Finland) and the LUMI consortium through a EuroHPC Extreme Access call, EHPC-EXT-2023E02-067.

References

[1] S. Pratt, E. Sangaline, P. Sorensen, H. Wang, Constraining the Eq. of State of Super-Hadronic Matter from Heavy-Ion Collisions, Phys. Rev. Lett. 114 (2015) 202301. arXiv:1501.04042, doi:10.1103/PhysRevLett.114.202301.

[2] L.-G. Pang, K. Zhou, N. Su, H. Petersen, H. Stöcker, X.-N. Wang, An equation-of-state-meter of quantum chromodynamics transition from deep learning, Nature Commun. 9 (1) (2018) 210. arXiv:1612.04262, doi:10.1038/s41467-017-02726-3.

[3] M. Abdallah, et al., Measurement of the Sixth-Order Cumulant of Net-Proton Multiplicity Distributions in Au+Au Collisions at $\sqrt{s_{NN}} = 27$, 54.4, and 200 GeV at RHIC, Phys. Rev. Lett. 127 (26) (2021) 262301. arXiv:2105.14698, doi:10.1103/PhysRevLett.127.262301.

[4] Y. Aoki, G. Endrodi, Z. Fodor, S. Katz, K. Szabo, The Order of the quantum chromodynamics transition predicted by the standard model of particle physics, Nature 443 (2006) 675–678. arXiv:hep-lat/0611014, doi:10.1038/nature05120.

[5] S. Borsanyi, et al., Is there still any T_c mystery in lattice QCD? Results with physical masses in the continuum limit III, JHEP 1009 (2010) 073. arXiv:1005.3508, doi:10.1007/JHEP09(2010)073.

[6] A. Bazavov, T. Bhattacharya, M. Cheng, C. DeTar, H. Ding, et al., The chiral and deconfinement aspects of the QCD transition, Phys.Rev. D85 (2012) 054503. arXiv:1111.1710, doi:10.1103/PhysRevD.85.054503.

[7] S. Borsanyi, Z. Fodor, M. Giordano, S. D. Katz, D. Nogradi, A. Pasztor, C. H. Wong, Lattice simulations of the QCD chiral transition at real baryon density, Phys. Rev. D 105 (5) (2022) L051506. arXiv:2108.09213, doi:10.1103/PhysRevD.105.L051506.

[8] P. Braun-Munzinger, J. Wambach, The Phase Diagram of Strongly-Interacting Matter, Rev. Mod. Phys. 81 (2009) 1031–1050. arXiv:0801.4256, doi:10.1103/RevModPhys.81.1031.

[9] S. Borsanyi, Z. Fodor, J. N. Guenther, R. Kara, S. D. Katz, P. Parotto, A. Pasztor, C. Ratti, K. K. Szabo, The QCD crossover at finite chemical potential from lattice simulations, Phys. Rev. Lett. 125 (2020) 052001. arXiv:2002.02821.

[10] A. Andronic, P. Braun-Munzinger, K. Redlich, J. Stachel, Decoding the phase structure of QCD via particle production at high energy, Nature 561 (7723) (2018) 321–330. arXiv:1710.09425, doi:10.1038/s41586-018-0491-6.

[11] M. D'Elia, M.-P. Lombardo, Finite density QCD via imaginary chemical potential, Phys. Rev. D67 (2003) 014505. arXiv:hep-lat/0209146, doi:10.1103/PhysRevD.67.014505.

[12] P. de Forcrand, O. Philipsen, The QCD phase diagram for small densities from imaginary chemical potential, Nucl.Phys. B642 (2002) 290–306. arXiv:hep-lat/0205016, doi:10.1016/S0550-3213(02)00626-0.

[13] C. Bonati, M. D'Elia, M. Mariti, M. Mesiti, F. Negro, F. Sanfilippo, Curvature of the chiral pseudocritical line in QCD: Continuum extrapolated results, Phys. Rev. D92 (5) (2015) 054503. arXiv:1507.03571, doi:10.1103/PhysRevD.92.054503.

[14] M. Stephanov, Non-Gaussian fluctuations near the QCD critical point, Phys.Rev.Lett. 102 (2009) 032301. arXiv:0809.3450, doi:10.1103/PhysRevLett.102.032301.

[15] S. collaboration, Precision Measurement of (Net-)proton Number Fluctuations in Au+Au Collisions at RHIC (4 2025). arXiv:2504.00817.

[16] P. Isserstedt, M. Buballa, C. S. Fischer, P. J. Gunkel, Baryon number fluctuations in the QCD phase diagram from Dyson-Schwinger equations, Phys. Rev. D100 (7) (2019) 074011. arXiv:1906.11644, doi:10.1103/PhysRevD.100.074011.

[17] Y. Lu, F. Gao, Y.-x. Liu, J. M. Pawlowski, Finite density signatures of confining and chiral dynamics in QCD thermodynamics and fluctuations of conserved charges (4 2025). arXiv:2504.05099.

[18] D. Bollweg, D. A. Clarke, J. Goswami, O. Kaczmarek, F. Karsch, S. Mukherjee, P. Petreczky, C. Schmidt, S. Sharma, Equation of state and speed of sound of (2+1)-flavor QCD in strangeness-neutral matter at nonvanishing net baryon-number density, Phys. Rev. D 108 (1) (2023) 014510. arXiv:2212.09043, doi:10.1103/PhysRevD.108.014510.

[19] S. Borsanyi, Z. Fodor, J. N. Guenther, S. D. Katz, P. Parotto, A. Pasztor, D. Pesznyak, K. K. Szabo, C. H. Wong, Continuum-extrapolated high-order baryon fluctuations, Phys. Rev. D 110 (1) (2024) L011501. arXiv:2312.07528, doi:10.1103/PhysRevD.110.L011501.

[20] S. Borsányi, Z. Fodor, J. N. Guenther, R. Kara, P. Parotto, A. Pásztor, L. Pirelli, C. H. Wong, Chiral versus deconfinement properties of the QCD crossover: Differences in the volume and chemical potential dependence from the lattice, Phys. Rev. D 111 (1) (2025) 014506. doi:10.1103/PhysRevD.111.014506.

[21] C. Allton, M. Doring, S. Ejiri, S. Hands, O. Kaczmarek, et al., Thermodynamics of two flavor QCD to sixth order in quark chemical potential, Phys.Rev. D71 (2005) 054508. arXiv:hep-lat/0501030, doi:10.1103/PhysRevD.71.054508.

[22] S. Borsanyi, Z. Fodor, J. N. Guenther, P. Parotto, A. Pasztor, L. Pirelli, K. K. Szabo, C. H. Wong, QCD deconfinement transition line up to μB=400 MeV from finite volume lattice simulations, Phys. Rev. D 110 (11) (2024) 114507. arXiv:2410.06216, doi:10.1103/PhysRevD.110.114507.

[23] C. Bonati, M. D'Elia, M. Mariti, M. Mesiti, F. Negro, F. Sanfilippo, Roberge-Weiss endpoint at the physical point of $N_f = 2 + 1$ QCD, Phys. Rev. D93 (7) (2016) 074504. arXiv:1602.01426, doi:10.1103/PhysRevD.93.074504.

[24] P. J. Gunkel, C. S. Fischer, Locating the critical endpoint of QCD: Mesonic backcoupling effects, Phys. Rev. D 104 (5) (2021) 054022. arXiv:2106.08356, doi:10.1103/PhysRevD.104.054022.

[25] L. Adamczyk, et al., Bulk Properties of the Medium Produced in Relativistic Heavy-Ion Collisions from the Beam Energy Scan Program, Phys. Rev. C 96 (4) (2017) 044904. arXiv:1701.07065, doi:10.1103/PhysRevC.96.044904.

[26] A. Hasenfratz, D. Toussaint, Canonical ensembles and nonzero density quantum chromodynamics, Nucl. Phys. B371 (1992) 539–549. doi:10.1016/0550-3213(92)90247-9.

[27] C. Brown, A. Abdelfattah, S. Tomov, J. J. Dongarra, Design, optimization, and benchmarking of dense linear algebra algorithms on AMD gpus, in: 2020 IEEE High Performance Extreme Computing Conference, HPEC 2020, Waltham, MA, USA, September 22-24, 2020, IEEE, 2020, pp. 1–7. doi:10.1109/HPEC43674.2020.9286214.
URL https://doi.org/10.1109/HPEC43674.2020.9286214